ROBUST PLUG–IN ALGORITHM FOR ADAPTIVE CANCELLATION OF QUASI-PERIODIC DISTURBANCES IN WEB WINDING SYSTEMS

Yulin Xu, Michel de Mathelin & Dominique Knittel

University Louis Pasteur (Strasbourg I), ERT-Enroulement*, LSIIT UMR CNRS 7005
ENSPS, Parc d'Innovation, Bd. Sébastien Brant, 67400 Illkirch, FRANCE
tel: +33 (0)3 90 24 44 70 or 71 fax: +33 (0)3 90 24 44 80
e-mail: michel.demathelin@ensps.u-strasbg.fr,
dominique.knittel@ipst-ulp.u-strasbg.fr
http://eavr.u-strasbg.fr, http://ert-enroulement.u-strasbg.fr

Keywords: Adaptive algorithm, quasi-periodic disturbance, web winding systems, robustness analysis, eccentricity and non-circularity disturbance rejection.

Abstract

This paper presents a plug-in algorithm to compensate web tension disturbances caused by the eccentricity and the non-circularity of the reel and rolls in web winding systems. The disturbances generated by the non-circularity and eccentricity of the roll have a quasi-periodic form with a frequency that varies with the rotation speed of the roll. The algorithm is based on an estimation of the phase component and the quadrature phase component of the disturbance. Approximate harmonic analysis and parameter design are done. The stability and robustness of the algorithm are also discussed. The ability of the algorithm to reject quasi-periodic disturbances with slowly varying frequencies is shown through simulations on the physical model as well as with experimental results.

1 Introduction

The system under study is quite common in industry. The system has at least three motors (cf. Figure 1): an unwinder, a traction motor and a winder, and it presents the inherent difficulties of web transport systems. In web transport systems, roll eccentricity and non-circularity create tension disturbances that are periodic or quasi-periodic due to change of radius of the roll when the roll is on the winder or the unwinder. These disturbances may induce web break and folds or material damage. This paper focuses on removing the effect of these disturbances that are quasi-periodic (periodic with a slowly varying frequency) and whose amplitude and phase are unknown.

There exist several approaches to tackle periodic disturbance rejection problems. A well known approach is based on repetitive control principles (see, e.g., [3], [6]). This type of approach works well when the disturbances are periodic. However, it is not suitable when the disturbance's main frequency varies with time. A second approach is based on adaptive algorithms (see, e.g., [1], [2], [8]). This approach may work even if the frequency is changing with time. In our application (high speed web winding), the frequency of the disturbance is known but varies with time during operation. Furthermore, for practical industrial applications, it is interesting to design an algorithm that can be added to an existing industrial controller to estimate the parameters of the disturbance and to cancel it. Therefore, in this paper we propose a plug-in type algorithm based on the adaptive algorithm for noise cancellation [1].

This paper is organized as follows, the first section presents the model of the web transport system based on the laws of physics with the tension disturbance on the unwinding roll. An experimental validation of the model is also described. The second section presents the disturbance cancellation algorithm with harmonic analysis and parameter design. In the third section, the stability and robustness of the algorithm are analyzed. Finally, in the last section, simulation and experimental results are presented using this plug-in algorithm on the unwinder of a web transport system.

2 Model of the web transport system

2.1 Nonlinear nominal model

The tension model in web transport systems is based on Hooke's law, Coulomb's law, mass conservation law and the laws of motion for each rotating roll (see [4]). Figures 1 and 2 show a typical three motors system with winder, unwinder,

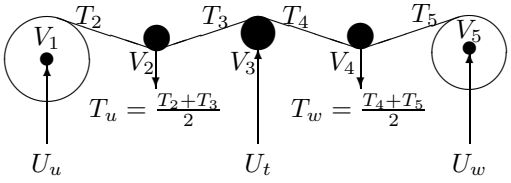

Figure 2: Three motors web transport system

tractor and two load cells that is used in our experiments. The complete model of this system is given by the following equa-

*supported by the French Ministry of Research through the project "Winding and high velocity handling of flexible webs" (ERT n^o 8, Contract 01 B-0395)

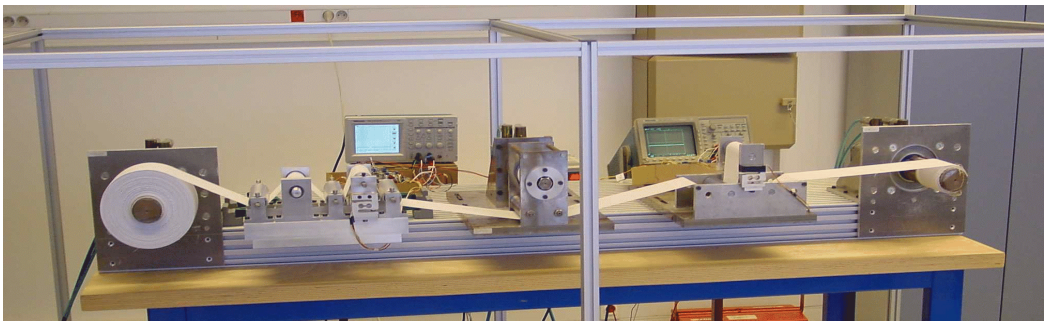

Figure 1: Three motors web winding system

tions (see, e.g., [4] and [5] for more details):
Tensions between consecutive rolls:

$$\begin{aligned} L_{k-1}\frac{dT_k}{dt} &= ES(V_k - V_{k-1}) + T_{k-1}V_{k-1} \\ &\quad -T_k(2V_{k-1} - V_k) \\ &\quad k = 2,3,4,5 \quad (V_k = R_k\Omega_k) \end{aligned} \tag{1}$$

where L_{k-1} is the web length between roll $k-1$ and roll k, T_k is the tension on the web between roll $k-1$ and roll k, V_k is the linear velocity of the web on roll k, Ω_k is the rotational speed of roll k, R_k is the radius of roll k, E is the Young modulus and S is the web section.
Laws of motion:
Unwinder: $(U_1 = U_u)$

$$\frac{d(J_1\Omega_1)}{dt} = R_1T_2 - K_1U_u - C_u - f_u\Omega_1 \tag{2}$$

Unwinder load cell:

$$J_2\frac{dV_2}{dt} = R_2^2(T_3 - T_2) - f_2V_2 \tag{3}$$

Tractor: $(U_3 = U_t)$

$$J_3\frac{d\Omega_3}{dt} = R_3(T_4 - T_3) + K_3U_t - C_t - f_t\Omega_3 \tag{4}$$

Winder load cell:

$$J_4\frac{dV_4}{dt} = R_4^2(T_5 - T_4) - f_4V_4 \tag{5}$$

Winder: $(U_5 = U_w)$

$$\frac{d(J_5\Omega_5)}{dt} = -R_5T_4 + K_5U_w - C_w - f_w\Omega_5 \tag{6}$$

where C_w, C_t, C_u are the dry friction torques of the three motors, respectively, f_u, f_2, f_t, f_4 and f_w are the viscous friction parameters, and K_kU_k are the motor torques. We can notice at this point that the inertia J_k and the radius R_k of the winder (k=1) and the unwinder (k=5) are time dependent and may vary on a large scale during the process operation (about 300 % for the radius in our experiments).

2.2 Eccentricity and non-circularity of the unwinder roll

The effect of the eccentricity and non-circularity of roll k can be modeled as a sinusoidal disturbance on the nominal radius of roll k:

$$R_k(t) = R_{k0}(t) + \sum_{m=1}^{\infty} A_{km}sin(\theta_{km}(t)) \tag{7}$$

where $R_{k0}(t)$ is the nominal radius of roll k and

$$\theta_{km}(t) = m\int_{t_0}^{t}\Omega_k d\tau + \delta\theta_{km}(t) \tag{8}$$

$\delta\theta_{km}(t)$ are the instantanous phases of the different harmonics. In a constant speed web transport system, if the eccentricity or non-circularity disturbance is due to the winder or the unwinder, the disturbance frequency is shifting with time due to the change of nominal radius of the roll.

2.3 Identification and experimental validation of the model

Firstly, the friction parameters of each motor are identified using a least squares method with data acquired at constant speed. Then, the inertia of the motors and the load cells as well as the torque gains are identified by a model matching method (cf. [7]). Measurements on the real system and simulations with the identified parameters are compared in Figure 3, in the case of a circular roll without eccentricity. Note that the difference at t=16 sec and t=36 sec is due to the slipping of the web that is not taken into account in the model. In the case of non-circularity or eccentricity disturbances, the difference between simulation and measurements can be seen in Figure 4. Indeed, if we look at the spectrum of the web tension measured during the winding process (cf. Figure 5), we can see that this disturbance is related to the winding and unwinding frequencies. The tension measured is the average tension between two consecutive rollers. We observe two fundamentals and two harmonics at frequencies which vary slowly during the winding process. The linear velocity is usually maintained constant in web transport systems, and the varying radius will modify the rotational speed of the winder and unwinder during the process operation (cf. equations (2) and (6)). The fundamentals in Figure 5

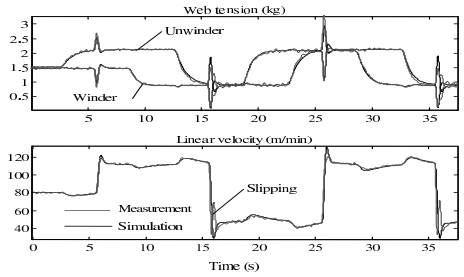

Figure 3: Simulation and measurement

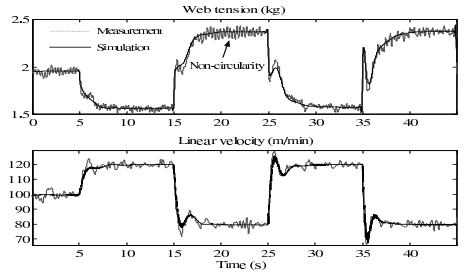

Figure 4: Simulation and measurement with a non-circular roll

correspond to the frequency of rotation of the unwinding and winding motors.

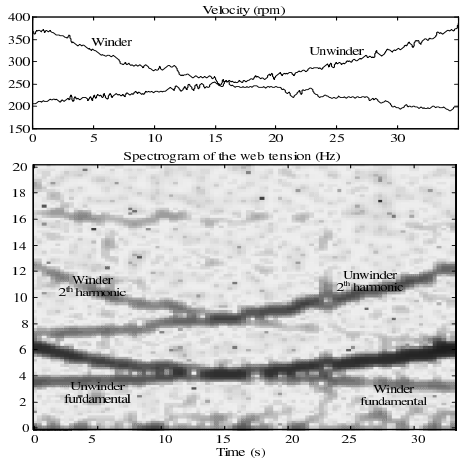

Figure 5: Experimental web tension spectrum

3 Disturbance rejection algorithm

The adaptive disturbance rejection algorithm is based on the estimation of the amplitude of two components of the disturbance that are in phase quadrature to each other. This algorithm is inspired from the work of Bodson (see, [1]) on noise cancellation. We adapt Bodson's approach to the case of a feedback control system with output signal y and reference input signal r. Another difference with Bodson's approach is that the central frequency Ω_c of the disturbance can be measured in our application and used at the input of the frequency modulator inside the algorithm. The adaptive algorithm scheme is shown

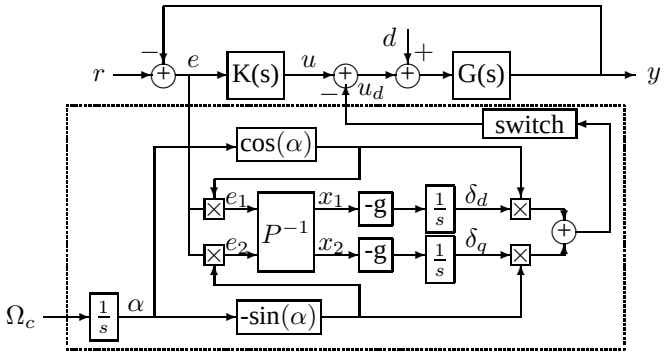

Figure 6: Adaptive algorithm scheme

in Figure 6 for the rejection of the first harmonic, where G(s) is the system, K(s) is the controller, and d is the unknown periodic disturbance. The estimate of the disturbance, u_d, is given by:

$$\begin{aligned} \dot{\alpha} &= \Omega_c \\ u_d &= \delta_d cos(\alpha) - \delta_q sin(\alpha) \end{aligned} \tag{9}$$

It's important that the disturbance cancellation algorithm does not make matter worse even during a starting transient. Therefore, Bodson's algorithm is modified by introducing a saturation on the estimated disturbance and a switching algorithm that can slowly close or open the disturbance cancellation loop.

3.1 Approximate harmonic analysis

An approximate harmonic analysis of this adaptive algorithm will allow us to deduce a simple design rule for the matrix P^{-1} and the gain g. The analysis of the adaptive scheme is based on the following assumption:

- The disturbance to be cancelled is equivalent to an input disturbance $d(t) = A_d(t)cos(\alpha_d(t))$.
- The value of Ω_c varies sufficiently slowly and the instantanneous frequency of the disturbance, $\omega_0 = \dot{\alpha}_d$, is sufficiently close to the known frequency Ω_c, so that $G(j\omega_0)$ can be replaced by $G(j\Omega_c)$.

We have:

$$\begin{aligned} y &= \frac{KG}{1+KG}[r] - \frac{G}{1+KG}[u_d - d] \\ e &= \frac{1}{1+KG}[r] + \frac{G}{1+KG}[u_d - d] \end{aligned} \tag{10}$$

Let's define:

$$G_R = Re[\frac{G}{1+KG}(j\Omega_c)] \qquad G_I = Im[\frac{G}{1+KG}(j\Omega_c)]$$

If we neglect the transient due to the variations of Ω_c, then

$$\begin{aligned} e \simeq\ & \frac{1}{1+KG}[r] + \delta_d G_R cos(\alpha) - \delta_d G_I sin(\alpha) \\ & -\delta_q G_R sin(\alpha) - \delta_q G_I cos(\alpha) - A_d G_R cos(\alpha_d) \\ & +A_d G_I sin(\alpha_d) \end{aligned} \tag{11}$$

If the high-frequency components are neglected due to the low-pass filtering of the signals e_1 and e_2, then,

$$\begin{bmatrix} e_1 \\ e_2 \end{bmatrix} \simeq P \begin{bmatrix} \delta_d - A_d cos(\alpha - \alpha_d) \\ \delta_q + A_d sin(\alpha - \alpha_d) \end{bmatrix} \quad (12)$$

where P is defined as:

$$P = \frac{1}{2} \begin{bmatrix} G_R & -G_I \\ G_I & G_R \end{bmatrix} \quad (13)$$

Therefore, the dynamics of δ_d and δ_q are decoupled as shown in the linearized model of the disturbance cancellation loop in Figure 7. The parameter, g, sets the estimation dynamics. In-

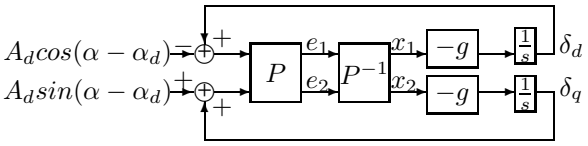

Figure 7: Linearized model

deed:

$$\begin{bmatrix} \dot{\delta}_d \\ \dot{\delta}_q \end{bmatrix} = -g \begin{bmatrix} \delta_d - A_d cos(\alpha - \alpha_d) \\ \delta_q + A_d sin(\alpha - \alpha_d) \end{bmatrix} \quad (14)$$

Therefore, g must be smaller than Ω_c in order to filter the high-pass frequency components, but large enough in order to follow the phase variations of the perturbation d. In that case, δ_d exponentially converges toward $A_d cos(\alpha - \alpha_d)$ and δ_q toward $-A_d sin(\alpha - \alpha_d)$, so that u_d exponentially converges toward d (with time constant $\frac{1}{g}$).

4 Robustness and stability analysis

In (12), P is the true plant matrix, while P^{-1} in Figure 6 is identified from the Bode plot. Therefore, there is always an error between both terms that may cause system unstability.
Let $P_\Delta = \hat{P} - P$, with

$$\hat{P} = \frac{1}{2} \begin{bmatrix} \hat{G}_R & -\hat{G}_I \\ \hat{G}_I & \hat{G}_R \end{bmatrix} \quad (15)$$

Considering the linearized scheme with uncertainty in Figure 8, we have

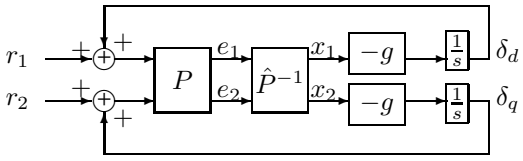

Figure 8: Linearized model with uncertainty

$$\dot{\delta} = -g(I + \Delta)(\delta + r) \quad (16)$$

where,

$$r = \begin{bmatrix} r_1 \\ r_2 \end{bmatrix} \qquad \delta = \begin{bmatrix} \delta_d \\ \delta_q \end{bmatrix} \qquad \Delta = -\hat{P}^{-1} P_\Delta$$

Whereupon, the *stability condition* for the linear system (16) is:

$$Re\{\lambda_i\{I + \Delta\}\} > 0 \quad \Leftrightarrow \quad Re\{\lambda_i\{\Delta\}\} > -1 \quad (17)$$

with

$$\begin{aligned} \Delta &= -\hat{P}^{-1} P_\Delta \\ &= -\frac{1}{\hat{G}_R^2 + \hat{G}_I^2} \begin{bmatrix} \hat{G}_R & \hat{G}_I \\ -\hat{G}_I & \hat{G}_R \end{bmatrix} \begin{bmatrix} G_{R\Delta} & -G_{I\Delta} \\ G_{I\Delta} & G_{R\Delta} \end{bmatrix} \\ &= -\frac{1}{\hat{G}_R^2 + \hat{G}_I^2} \begin{bmatrix} a & -b \\ b & a \end{bmatrix} \end{aligned}$$

where $a = \hat{G}_R G_{R\Delta} + \hat{G}_I G_{I\Delta}$ and $b = \hat{G}_R G_{I\Delta} - \hat{G}_I G_{R\Delta}$, then

$$\lambda_i\{\Delta\} = \frac{a \pm jb}{\hat{G}_R^2 + \hat{G}_I^2} \qquad i = 1, 2 \quad (18)$$

So that (17) is equivalent to

$$\frac{\hat{G}_R G_{R\Delta} + \hat{G}_I G_{I\Delta}}{|\hat{G}|^2} < 1 \quad (19)$$

with $\hat{G}_R = G_R + G_{R\Delta}$, $\hat{G}_I = G_I + G_{I\Delta}$, and equation (19) becomes:

$$\frac{\hat{G}_R G_R + \hat{G}_I G_I}{|\hat{G}|^2} > 0 \quad (20)$$

Let $\frac{\hat{G}_R}{|\hat{G}|} = cos\varphi$ and $\frac{\hat{G}_I}{|\hat{G}|} = sin\varphi$, then the following stability condition can be deduced:

$$G_R cos\varphi + G_I sin\varphi > 0 \quad (21)$$

This condition is shown as the shaded area in Figure 9 which is defined by an orthogonal line which goes though the origin to the vector $\hat{G}$, i.e, if G is in the shaded area, then the algorithm will be stable. In other words, if G and $\hat{G}$ are in the same half plant limited by the orthogonal line to $\hat{G}$, the algorithm is stable.

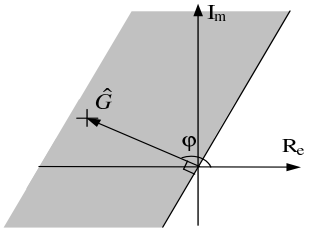

Figure 9: Stability condition

5 Application to the web winding system

In the web winding and transport system, if the eccentricity and non-circularity disturbances are due to roll k, then the main tension disturbance essentially is on tension T_{k+1}. Therefore, we add the adaptive algorithm on the controller of the motor of roll k with a feedback of the tension T_{k+1}. For exemple, if the disturbance is due to the unwinder, we add the adaptive disturbance cancellation algorithm on the unwinder controller as shown in Figure 10.

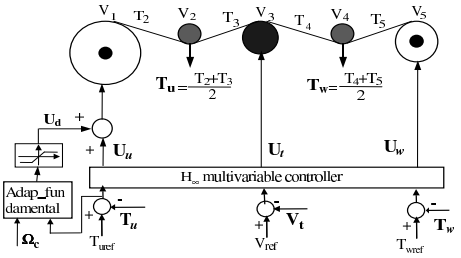

Figure 10: Control scheme with adaptive algorithm on the unwinder

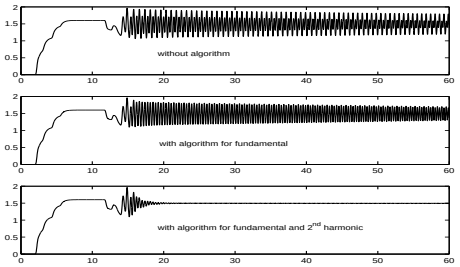

Figure 13: Simulation with algorithms for harmonics

5.1 Selection of design Parameters

a) Parameter g: In our simulations and experiments, $\Omega_c \in [8.6, 50]$ rad/s and parameter $g = 1 \sim 10$.
b) System matrix P: The Bode plot of the transfer function between the control signal of the unwinder u_d and the measured torque error, $T_{uref} - T_u$, is shown in Figure 11 for different constant reference linear velocities V_{ref} of the web. Based on the value of V_{ref}, an average value $\bar{\Omega}_c$ is computed for Ω_c and the corresponding matrix P (cf. equation(13)) is measured on the Bode plot.

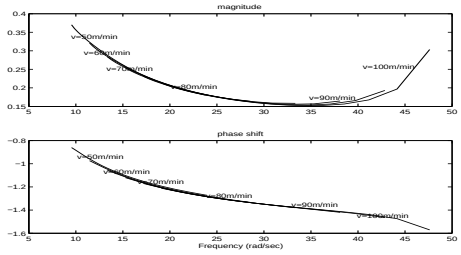

Figure 11: Bode plot of the transfer between u_d to $T_{uref} - T_u$

5.2 Simulations with the adaptive algorithm

We demonstrate the validity of the adaptive algorithm through simulations with the algorithm at the unwinder roll as in Figure 10. Considering eccentricity or non-circularity disturbances on the unwinder, the tension on the unwinder and the winder is shown in Figure 12 with and without the adaptive algorithm. One can clearly see that the adaptive algorithm completely compensates the disturbances. Figure 13 shows that two harmonics on the unwinder can be also cancelled by two parallel algorithms (one algorithm with central frequency Ω_c and the other with central frequency $2\Omega_c$).

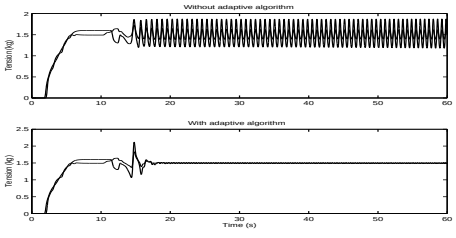

Figure 12: Simulation of adaptive algorithm

5.3 Experimental results

In our practical system, the main controller is a H_∞ multivariable controller (see [5]). One or more adaptive plug-in algorithms are added to this real system. Figure 14 shows the spectrogram (amplitude of the Fourier transform with a sliding window) of the measured web tension at the unwinder during a real experiment on the system shown in Figure 1 for an unwinder roll which presents an eccentricity and a noncircularity at the web transport speed $V_{uref} = 50$ m/min. For this experiment, the adaptive disturbance cancellation algorithm is not added. Figure 15 shows the spectrogram of the measured web tension at the unwinder during a real experiment at the web transport speed $V_{uref} = 50$ m/min with the adaptive disturbance

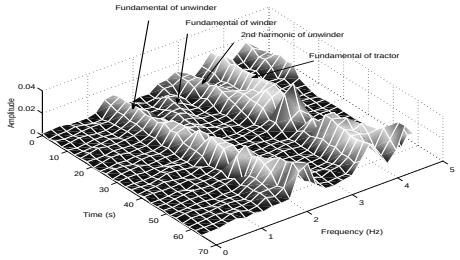

Figure 14: Spectrogram of tension measurement at 50 m/min without disturbance rejection algorithm

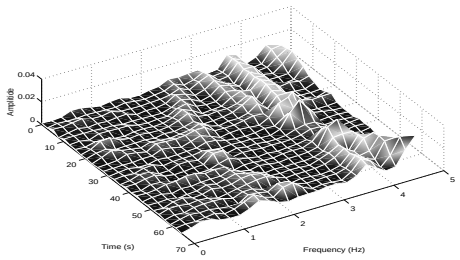

Figure 15: Spectrogram of tension measurement at 50 m/min with algorithm

cancellation algorithm on the unwinder. One can see that the slowly varying first harmonic is almost completely cancelled. The higher frequency disturbance term is due to the traction motor. The experimental result can be seen in Figure 16 when

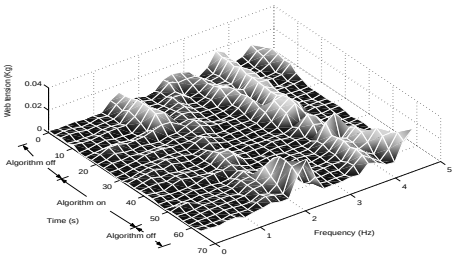

Figure 16: Spectrogram of tension measurement at 50 m/min with algorithm in a period

the adaptive algorithm is switched on between the time instants t=20 s and 50 s. During this time interval, the fundamental of the disturbance due to the unwinder is completely eliminated and the transient from activation to desactivation of the cancellation algorithm does not create oscillations of the tension.

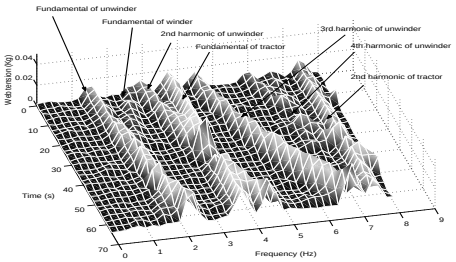

Figure 17: Spectrogram of tension measurement (fundamental and harmonics) at 50 m/min without disturbance rejection algorithm

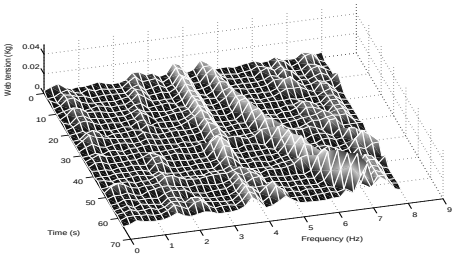

Figure 18: Spectrogram of tension measurement (fundamental and harmonics) at 50 m/min with algorithm (rejection of fundamental and 2nd harmonic)

If there exist more harmonics on the unwinder, several algorithms can be added in parallel on the experimental system. Figure 17 shows the spectrogram with several harmonics of the measured tension without disturbance rejection algorithm. Then, in Figure 18, the rejection of disturbances is activated for the fundamental and also for the second harmonic. Comparing both figures, we can notice that the adaptive rejection algorithm is effective to eliminate both the fundamental and the harmonic. Moreover, the measurements show also that even higher harmonics are simultaneously attenuated.

6 Conclusion

In this paper, an adaptive algorithm is proposed to reject the disturbances generated by the non-circularity and eccentricity of the rolls in web transport systems. It estimates the disturbances based on the tension error signals in the system and cancels them. This adaptive algorithm works when the frequencies of the disturbance are known and vary slowly. The stability robustness analysis of the algorithm is given and one can clearly see that the adaptive algorithm is robust for quasi-periodic disturbance rejection. Simulations with the physical model and practical experiments on a 3-motors web transport system verify the theoretical results of the analysis and show the usefulness of the algorithm for the rejection of quasi-periodic disturbances. Finally, it should be noted that the algorithm is plug-in in nature and can be added on an existing scheme.

References

[1] M. Bodson, S. C. Douglas. “Adaptive algorithms for the rejection of sinusoidal disturbances with unknown frequency”, *Automatica*, **33** (12), pp. 2213–2221, (1997).

[2] M. Bodson, J. S. Jensen, S. Douglas. “Active noise control for periodic disturbances”, *IEEE Transactions on Control Systems Technology*, **9** (1), pp. 200–205, (2001).

[3] G. Hillerström. “Adaptive suppression of vibrations–a repetitive control approach”, *IEEE Transactions on control Systems Technology*, **4** (1), pp. 72–78, (1996).

[4] H. Koç. “Modélisation et commande robuste d’un système d’entrainement de bande flexible”, Ph.D. thesis, *Université Louis Pasteur (Strasbourg I University)*, (2000).

[5] H. Koç, D. Knittel, M. de Mathelin, G. Abba. “Modeling and robust control of winding systems for elastic webs”, *IEEE Transactions on Control Systems Technology*, **10** (2), pp. 197–208, (2002).

[6] M.-C. Tsai, W.-S. Yao. “Design of a plug-in type repetitive controller for periodic inputs”, *IEEE Transactions on Control Systems Technology*, **10** (4), pp. 547–555, (2002).

[7] E. Walter, L. Pronzato. “Identification of parametric models from experimental data”, *Springer*, (1997).

[8] Y. Xu. “Robust cancellation of eccentricity and noncircularity tension disturbances in web winding systems”, Ph.D. thesis, *Université Louis Pasteur (Strasbourg I University)*, (2003).